

1 Comprehensive single-cell atlas of the mouse retina

2
3 Jin Li^{1,2,*}, Jongsu Choi^{3,*}, Xuesen Cheng^{1,2,*}, Justin Ma⁴, Shahil Pema¹, Joshua R. Sanes⁵,
4 Graeme Mardon^{1,4,6}, Benjamin J. Frankfort⁶, Nicholas M. Tran¹, Yumei Li^{1,2}, Rui Chen^{1,2,3}

5
6 1. Department of Molecular and Human Genetics, Baylor College of Medicine, Houston,
7 Texas 77030, USA.

8 2. Human Genome Sequencing Center, Baylor College of Medicine, Houston, Texas 77030,
9 USA.

10 3. Department of Biochemistry and Molecular Biology, Baylor College of Medicine, Houston,
11 Texas 77030, USA.

12 4. Department of Pathology and Immunology, Baylor College of Medicine, Houston, Texas
13 77030, USA.

14 5. Center for Brain Science and Department of Molecular and Cellular Biology, Harvard
15 University, Cambridge, Massachusetts 02130, USA.

16 6. Departments of Ophthalmology and Neuroscience, Baylor College of Medicine, Houston,
17 Texas 77030, USA.

18
19 *These authors contributed equally to this work.

20 Corresponding author: Rui Chen (ruichen@bcm.edu)

21 Abstract

22
23 Single-cell RNA sequencing (scRNA-seq) has advanced our understanding of cellular
24 heterogeneity at the single-cell resolution by classifying and characterizing cell types in
25 multiple tissues and species. While several mouse retinal scRNA-seq reference datasets have
26 been published, each dataset either has a relatively small number of cells or is focused on
27 specific cell classes, and thus is suboptimal for assessing gene expression patterns across all
28 retina types at the same time. To establish a unified and comprehensive reference for the
29 mouse retina, we first generated the largest retinal scRNA-seq dataset to date, comprising
30 approximately 190,000 single cells from C57BL/6J mouse whole retinas. This dataset was
31 generated through the targeted enrichment of rare population cells via antibody-based
32 magnetic cell sorting. By integrating this new dataset with public datasets, we conducted an
33 integrated analysis to construct the Mouse Retina Cell Atlas (MRCA) for wild-type mice, which
34 encompasses over 330,000 single cells. The MRCA characterizes 12 major classes and 138 cell
35 types. It captured consensus cell type characterization from public datasets and identified
36 additional new cell types. To facilitate the public use of the MRCA, we have deposited it in
37 CELLxGENE, UCSC Cell Browser, and the Broad Single Cell Portal for visualization and gene
38 expression exploration. The comprehensive MRCA serves as an easy-to-use, one-stop data
39 resource for the mouse retina communities.

40 Introduction

41
42 The retina is a highly heterogenous part of the eye that captures and processes the
43 light signal¹⁻³. The processing is enabled through five classes of retinal neurons:
44 photoreceptors (PR), horizontal cells (HC), bipolar cells (BC), amacrine cells (AC), and retinal
45 ganglion cells (RGC), which form an intricate circuitry necessary for processing and relaying
46 the light signal to the visual cortex. Non-neuronal cells such as Müller glia cells (MG), microglia,
47 astrocytes, and retinal pigment epithelial cells (RPE) provide structural integrity of the tissue
48 and carry out various supporting roles such as metabolism and neuronal homeostasis in the
49 retinal microenvironment^{4,5}. Characterization of distinct retinal cell types is, therefore, critical
50 in advancing our understanding of the fine intricacies of cell interactions involved in retinal
51 biology and visual disorders.

52 Single cell technologies have opened a window into knowledge of cellular
53 heterogeneity and intricate cell-to-cell interactions that cannot currently be resolved at the
54 tissue level and have allowed exploration of individual cellular expression signatures, which
55 can be mapped to unique molecular cell types^{6,7}. The resulting cell atlas can serve as a
56 foundation for numerous applications, including the annotation of cell types in other scRNA-
57 seq experiments⁸, the identification of differentially expressed targets for purification or
58 manipulation⁹, and the generation of marker panels useful for single-molecule imaging,
59 including spatial profiling¹⁰. While studies have demonstrated cell type heterogeneities in
60 various tissues, several perplexing issues remain to be addressed in establishing a
61 comprehensive cell atlas such as the agreement on cell type definitions across different
62 experiments or whether enough cells have been profiled to exhaust all existing cell types.
63 Integrated analyses of various scRNA-seq datasets from different studies, therefore, can
64 provide an important insight that comprehensively addresses such issues.

65 The mouse retina provides an important model for the study of neurobiology, with
66 more than 130 distinct cell types characterized through previous scRNA-seq studies^{7,9,11-15}.
67 However, the scRNA-seq datasets have been generated separately for BC¹¹, AC¹², and RGC
68^{9,13,14}, with the largest dataset containing just under 36,000 cells, making it difficult to use in
69 aggregate. Though most of these datasets are independently browsable on the Broad Single
70 Cell Portal¹⁶ and accessible through separate databases such as the Gene Expression Omnibus
71 (GEO) repository, it can be challenging to assess gene expression patterns across all retinal cell
72 types. Ensuring these atlases define a complete set of retinal cell types remains a major
73 challenge that can only be addressed by powering studies to sufficiently profile the rarest
74 retinal cell types. Here, we generated scRNA-seq data of over 189,000 cells in the mouse retina
75 to complement 141,000 cells from six publicly available scRNA-seq datasets^{9,11-15}, creating a
76 unified cell atlas of the wild-type mouse retina containing over 330,000 cells. Our integrated
77 analysis presents a comprehensive characterization of all major cell classes in the retina,
78 including non-neuronal types, as well as a consensus cell type annotation of BCs, ACs, and
79 RGCs. Accessible, interactive web browsers have facilitated easy visualization of atlas
80 characterizations and exploration of gene expression in the MRCA. The comprehensive unified
81 MRCA will serve as a valuable resource for the community.

82

83 **Results**

84

85 ***Generation of scRNA-seq dataset for wild-type mouse retina***

86 To establish a comprehensive atlas of the mouse retina, we performed scRNA-seq
87 profiling with C57BL/6J mouse retina tissue samples, aged from P14 to 12 months, for over
88 189,000 cells (**Fig. 1a** and Methods). As summarized in **Table 1**, six samples of varying ages
89 were dissociated retinal cells without enrichment, and ten samples of eight weeks old were
90 enriched using surface markers CD73 and CD90.1 to enrich for rare cell population. Depletion
91 of rod photoreceptors was achieved by removing cells positive for CD73 using anti-CD73-PE
92 antibody and anti-PE magnetic beads, which primarily label photoreceptor precursors and
93 mature rod photoreceptors in mice^{12,17}. To enrich ACs and RGCs, CD90.1 positive cells are
94 selected^{18,19}.

95

96 ***Integration of scRNA-seq datasets for the mouse retina***

97 To compile the most comprehensive scRNA-seq data for the MRCA, we curated and
98 obtained six publicly available scRNA-seq datasets, each enriched for a specific cell type using
99 transgenic labels or immunolabeling combined with FACS. Together, they consisted of over
100 141,000 cells. To consolidate the transcript annotation between different datasets, we used
101 the Cell Ranger (version 7.0.1) pipeline to align raw FASTQ files from four datasets obtained
102 from GEO and Sequence Read Archive (SRA) repositories. Count matrices of these datasets

103 were generated using the mm10 reference genome obtained from 10x Genomics
104 (<https://cf.10xgenomics.com/supp/cell-exp/refdata-gex-mm10-2020-A.tar.gz>). Five of the
105 published studies were sequenced on the 10x Genomics 3' platform, and one (Shekhar *et al.*)
106 was generated using the Drop-seq protocol⁷. The Drop-seq data were aligned against mm10
107 and processed into count matrices using the Drop-seq pipeline
108 (<https://github.com/broadinstitute/Drop-seq>). The cell type labels of previous annotations
109 were obtained from the Broad Single Cell Portal website¹⁶. To remove technical variations
110 introduced across different experiments or studies, scVI²⁰ was applied to integrate all newly
111 generated and public datasets, generating a low-dimensional representation (**Fig. 1b** and
112 Methods). Putative cell doublets were further removed using the deep learning doublet
113 identification method Solo²¹ (**Supplementary Fig. 1a**).

114 In the integrated data, the public dataset accounts for 43%, while the newly generated
115 data accounts for the remaining 57% (**Fig. 1c**). Within the integrated UMAP, 97 clusters were
116 identified (**Supplementary Fig. 1b**). These clusters were annotated as one of 12 major classes,
117 including PR, BC, AC, RGC, HC, MG, RPE, astrocyte, microglial, endothelial, and pericyte, using
118 known marker gene expression^{22,23} (**Supplementary Fig. 1c**). Cells from non-enriched retina
119 samples showed a distribution across major classes at an expected proportion, with rod
120 photoreceptors as the biggest proportion². In contrast, enriched samples from both newly
121 generated data and previous studies showed the expected skewed distribution of cell types in
122 BCs, ACs, and RGCs (**Supplementary Fig. 1d**). The two newly generated samples with
123 enrichment methods, CD73⁻ and CD90.1⁺ samples, were primarily composed of BCs and ACs,
124 respectively, contributing to 83% (122.6K out of 147.7K) and 25% (11.2K out of 44K) of all BCs
125 and ACs in the integrated data, respectively.

126 Previous studies have identified 15 distinct types of BCs, 64 ACs, and 46 RGCs^{9,11,12}. To
127 determine the consensus annotation of neuronal types for these subclasses, we performed
128 clustering analysis at higher resolution within individual BC, AC, and RGC classes (**Fig. 1d** and
129 **Fig. 1e**).

130

131 **15 types of bipolar cells**

132 A total of 147,700 BCs were identified in the integrated datasets, with 122,600 cells
133 from our newly generated CD73⁻ sample and 19,800 cells from the Shekhar *et al.* study¹¹. The
134 integrated analysis identified 15 BC clusters, corresponding to previously annotated BC types
135 (**Fig. 2a-b** and Methods). The 15 clusters of integrated BCs showed a generally even
136 distribution of cells from various samples, with the exception of two types, BC1A and BC1B,
137 where more than 90% of populations came from the study by Shekhar *et al.* possibly due to
138 differences in enrichment methods (**Fig. 2a, 2d** and **Supplementary Fig. 2d-e**). The final
139 annotation of BCs revealed consistent expression profiles of previously identified BC type
140 marker genes^{11,24} (**Fig. 2b-c**). With a significant addition of BCs in the MRCA, clear separation
141 of BC8 and BC9 is observed, which were merged but demonstrated substructure in the
142 Shekhar *et al.* dataset (**Fig. 2a-b**). The separate clusters showed proper expression patterns of
143 known markers like *Cpen9* in BC9^{11,25}. In addition, additional BC type markers were identified
144 via differential gene expression analysis, which showed more specific expressions than
145 previous marker genes, such as *Tafa4* in BC4, *Ptppt* in BC5A, and *Gm13986* in BC8 (**Fig. 2e**).
146 Interestingly, despite an almost ten-fold increase in the number of BCs in our analysis, we did
147 not observe any sign of a novel cell type, which suggests that the mature mouse retina likely
148 only contains 15 BC types.

149

150 **Amacrine cells**

151 Through CD90.1 positive enrichment, the newly generated samples contributed
152 11,200 ACs, in addition to the 27,600 ACs from Yan *et al.*¹² in the integrated dataset
153 (**Supplementary Fig. 3a-b**). Utilizing the collected data, the integrated analysis annotated 63
154 AC types, revealing consistent expression profiles of known marker genes (**Fig. 3a-b** and

155 Methods). While a minimal batch effect in each cluster was observed across different sample
156 sources, CD90.1⁺ and Ma *et al.* RGC samples showed biased enrichment towards GABAergic
157 types except for AC4, AC10, and AC28 (**Supplementary Fig. 4e**). The bias in cell type population
158 appears to be directly tied to the preferential expression of *Thy1* (CD90) in sub-populations of
159 ACs (**Supplementary Fig. 4d**). In particular, *Thy1* is characterized as being expressed primarily
160 in GABAergic AC types ²⁶.

161 The integrated analysis of ACs demonstrated that four types, AC18, AC20, AC36, and
162 AC45, have been previously under-clustered, each splitting into two clusters in the integrated
163 UMAP (**Fig. 3c**). AC18, which expresses *Cck* neuropeptide ²⁷, is split into C24 and C27 in our
164 clustering and has been labeled as AC18A and AC18B in the final annotation (**Fig. 3d**).
165 Interestingly, the cell type marker *Cck* is highly expressed in AC18A, but not in AC18B
166 (**Supplementary Fig. 5a**). AC20, which does not contain any known marker, is divided into C42
167 and C60 (AC20A and AC20B), with its marker *Sema3a* also expressed highly in AC20A, but not
168 in AC20B (**Supplementary Fig. 5b**). A non-GABAergic non-glycinergic (nGnG) type 4, AC36, is
169 split into C58 and C61 (AC36A and AC36B), consistent with previous finding of two
170 morphologically distinct AC36 types in the INL and displaced in the GCL, stratifying to S3 and
171 S5 sublaminae of the IPL ^{10,28}. By examining the list of differentially expressed genes (DEG)
172 between the two broadly isolated types ²⁸, we annotated AC36A as the S3 type by the
173 increased markers such as *Gbx2*, *Tac1*, and *Pcdh8* and AC36B as the S5 type by *Gad1*, *Gad2*,
174 and *Id4*. (**Fig. 3e**). Lastly, a catecholaminergic type 1 cell type ²⁹, AC45, is split into C64 and C66
175 (AC45A and AC45B). The expression of *Chl1*, which distinguishes catecholaminergic type 1
176 from type 2, was increased specifically in AC45A. The DEG analysis between the clusters of the
177 previously under-clustered cell type revealed many genes enriched specifically in each cluster,
178 with *Cck*, *Sema3a*, *Chl1* being one of the top-ranked genes in AC18A, AC20A and AC45A,
179 respectively (**Supplementary Fig. 5b**). Out of the four under-clustered cell types, only one,
180 AC20, showed a biased sample source from Yan *et al.* data. Furthermore, while cells from Yan
181 *et al.* were distributed across both AC45A and AC45B, AC45B contains an increased number of
182 cells from the newly generated CD90.1 sample (**Supplementary Fig. 4e**).

183 As a result, we have identified 67 AC types that can be grouped into four AC
184 subclasses: 49 GABAergic, 10 Glycinergic, 3 Both, and 5 nGnG ACs. Within the final dataset,
185 GABAergic ACs make up 67.7% of the total AC population, followed by Glycinergic ACs at
186 22.5%, GABA/Glycinergic ACs at 1%, and nGnG ACs at 8.7%. However, these distributions are
187 likely biased towards GABAergic ACs due to the inclusion of cells from CD90.1⁺ and CD90.2⁺
188 enriched collections.

189

190 **Retinal ganglion cells**

191 The integrated data contains 77,900 RGCs, primarily from the three publicly available
192 datasets. The integration of the collected data identified all 46 previously identified RGC types
193 (**Fig. 4a** and Methods). Examination of known cell type markers in the integrated data with the
194 final annotation showed proper expression profiles in corresponding types ^{9,18,30} (**Fig. 4b**).
195 Although no novel cluster was identified, our integrated analysis of RGCs similarly identified
196 the division of two cell types, 16_ooDS_DV (ON-OFF direction-selective dorsal and ventral) and
197 18_Novel, into distinct clusters (**Fig. 4c**). The 16_ooDS_DV, which contains both types with
198 dorsal and ventral orientation selective functional roles ^{31,32}, was split into C31 and C39, similar
199 to the supervised clustering analysis done in the Tran *et al.* ⁹, Jacobi *et al.* ¹³, and Ma *et al.* ¹⁴
200 studies. Examination of the marker genes *Calb1* and *Calb2* demonstrated that C39 is the
201 ventral selective type with high expression of *Calb2*, and C31 is the dorsal selective type with
202 *Calb1* expression ⁹. In addition, the 18_Novel type could also be split into C36 and C40.
203 Interestingly, while C40 contained only cells with 18_Novel labels, C36 contained a mixture of
204 18_Novel and 44_Novel labels (**Supplementary Fig. 7a-c**). The same annotation improvements
205 were also observed in Ma *et al.* ¹⁴. Examination of 18_Novel markers *Pcdh20* and
206 *4833424E24Rik* revealed increased expression of both markers in C40, yet *Pcdh20* expression

207 was absent in C36 (**Supplementary Fig. 7e**). The DEG analysis further demonstrated many
208 genes selectively expressed in these two clusters (**Supplementary Fig. 7d**). In total, we have
209 identified 47 RGC types in the MRCA (**Fig. 4d**).

210

211 **Non-neuronal retinal cells**

212 To include the comprehensive set of cell types in the retina in the MRCA, 18,500 non-
213 neuronal cells were integrated for six non-neuronal cell types, including astrocyte, endothelial,
214 MG, microglia, pericyte, and RPE (**Supplementary Fig. 8a** and **Fig. 1e**). These cells are evenly
215 distributed in the collected datasets, except for astrocytes solely from the Benhar *et al.* dataset
216 ¹⁵ (**Supplementary Fig. 8b**). After being combined with neuronal retinal cells, the MRCA
217 consisted of 12 major classes and 138 cell types.

218

219 **Data dissemination at accessible interactive web browsers**

220 The MRCA has been made available for public access using the CELLxGENE platform
221 (<https://cellxgene.cziscience.com/collections/a0c84e3f-a5ca-4481-b3a5-ccfda0a81ecc> and
222 <https://mouseatlas.research.bcm.edu/>) (**Fig. 5a-c**). The MRCA is also accessible on UCSC Cell
223 Browser (<https://retina.cells.ucsc.edu>) and the Broad Single Cell Portal. Pre-computed gene
224 expression profiles of all cells included in the integrated analysis can be examined and
225 visualized. Users also have access to the metadata information, including major class and cell
226 type labels in the database. The accessible interactive web browsers of the MRCA can aid in
227 easy access to the transcriptome profiles of any given mouse retinal cells without the
228 bioinformatic burden and provides a valuable tool for the vision community.

229

230 **Discussion**

231 As part of the central nervous system, the retina contains numerous neuronal types
232 with distinct morphologies and functional roles ^{1,33}. The heterogenous cell type composition
233 and the stereotypically patterned structure of the tissue makes the retina an ideal model for
234 single-cell sequencing studies in establishing the single-cell atlas ^{7,22,34}. Although several
235 scRNA-seq studies focusing on the retina tissue have been done previously ^{7,9,11-15}, each
236 available dataset contains single-cell profiles primarily of one or a few retinal cell classes with
237 a limited number of cells. Furthermore, no systematic evaluation or comparison of the
238 datasets has been done yet to cross-validate the cell type transcriptomes and address
239 annotation consensus.

240 In this study, we generated scRNA-seq profiles of 189,000 retinal cells from 16 scRNA-
241 seq experiments to perform an integrated analysis with 141,000 retinal cells from six
242 previously reported datasets. Six out of the newly generated collections were done using
243 endogenous retina tissues with simple dissociation and without enrichment. Photoreceptors
244 constitute over 70% of the cell proportion in the retina ^{2,35}, and there are only two subclasses
245 of photoreceptors, which are well studied. Therefore, we utilized two methods for rare
246 population cell type enrichment. The first way was depleting the rod photoreceptors. To
247 achieve this goal, the rod photoreceptor cell surface marker, CD73, was used in seven of the
248 16 experiments. Though this marker is generally considered as a specific marker for rod
249 photoreceptors, it is also expressed on the surface of a subset of ACs, HCs, and MGs. Depletion
250 increased the enrichment of BCs from 12% to 90%. Furthermore, CD90.1 was used to enrich
251 certain retinal neurons such as ACs and RGCs in three experiments. Enrichment of retinal cells
252 with CD90.1 also showed an increased number of ACs with some RGCs.

253 One of the challenges in integrating and comparing publicly available data is that they
254 are generated using different single-cell experimental platforms and analysis pipelines ^{36,37}.
255 One public data enriched with BCs from Shekhar *et al.* ¹¹ was generated using the Drop-seq ⁷
256 technology and was processed separately using the Cell Ranger transcript annotation. The four
257 other sources of publicly available data were done using the 10x Genomics platform. A minimal
258 batch effect across data sources was observed in the integrated analysis, with the expected

259 distribution and clustering of major classes from corresponding sources. While the newly
260 generated data without enrichment were primarily composed of rod photoreceptors, cells
261 from the newly generated data with enrichment and publicly available data showed a proper
262 distribution across BCs, AC, and RGCs.

263 Integrated analysis of various scRNA-seq datasets allowed us to examine AC, BC, and
264 RGC types, which together comprise over 100 distinct cell types. Through the integrated
265 analysis, we addressed two key questions on the neuronal cell types in the retina: to confirm
266 the consensus cell type signatures and to examine whether the total number of cell types of
267 retinal neurons is exhausted. Following the initial integrated analysis to identify major classes,
268 subsets of each major class were subjected to further integration and two-level clustering to
269 annotate all previously identified cell types, which showed an even distribution of data sources
270 in general. The cell type annotation was achieved through examining known marker gene
271 expressions and previous annotation labels when available. Although our newly generated
272 data resulted in a significantly increased number of cells in the integrated analysis of BCs, ACs,
273 and RGCs, we did not observe significant increases of novel cluster. As such, the previously
274 reported set of BC types in the adult mouse retina is likely complete, supported by the more
275 than 7-fold increase in BCs in the integrated data. On the other hand, our integrated analysis
276 updates annotations of AC and RGC types. In particular, we observed several instances of
277 previously under-clustered AC and RGC types splitting into distinct clusters in our analysis. For
278 example, we confirmed the separation of 16_ooDS_DV types into two distinct clusters in the
279 integrated data of RGCs, which was separated into dorsal and ventral selective types only
280 through supervised clustering in the Tran *et al.* study⁹ and later confirmed in Jacobi *et al.*¹³
281 study. Furthermore, we identified the separation of AC36 and assigned its clusters to S3 and
282 S5, stratifying *Gbx2*⁺ AC types²⁸, which strengthens our analysis by connecting to biologically
283 distinct cell types. The separation of previously merged cell types into distinct clusters can be
284 attributed to the increased number of cells in our integrated analysis. This suggests that, while
285 our AC and RGC type annotations are comprehensive, they will likely continue to be refined
286 by future studies.

287 Finally, we have deposited the MRCA into interactive web browsers that are user-
288 friendly and publicly accessible. This allows for the examination of raw and normalized gene
289 expression profiles of all retinal cells, along with their metadata such as major class and cell
290 type annotation. The MRCA not only provides the consensus signature of mouse retinal cell
291 types by comparing multiple scRNA-seq data but also alleviates the bioinformatics burden for
292 many vision researchers who wish to examine transcriptome signatures in any cell type of their
293 interest.

294

295 **Methods**

296

297 ***Generation of scRNA-seq datasets of the mouse retina***

298 We have generated 16 scRNA-seq samples of the mouse C57BL/6J retina (**Table 1**). All
299 mice were male. All procedures were approved by the Institutional Animal Care and Use
300 Committee (IACUC) and followed the Association for Research in Vision and Ophthalmology
301 (ARVO) Statements for the Use of Animals in Ophthalmic and Vision Research, in addition to
302 the guidelines for laboratory animal experiments (Institute of Laboratory Animal Resources,
303 Public Health Service Policy on Humane Care and Use of Laboratory Animals). After dissection,
304 retinas were dissociated into single cells using papain-based enzyme following the published
305 protocol³⁸. With activated 45U of papain (Worthington, Cat. #LS003126) solution (1mg L-
306 Cystine, Sigma; 8 KU of DNase I, Affymetrix; in 5 ml DPBS), retina was incubated at 37C for
307 ~20min, followed by the replacement of buffer with 2ml ovomucoid solution (15 mg
308 ovomucoid, Worthington Biochemical; 15 mg BSA Thermo Fisher Scientific; in 10 ml DPBS) and
309 500ul deactivated FBS. Following the enzymatic digestion step, the retina tissues were
310 carefully triturated and filtered using 20 um plastic meshes. Trituration steps were repeated

311 with additional 1ml ovomucoid solution until no tissue was visible. Single-cell suspension was
312 spun down at 300g, 4C for 10 min and used in the next step.

313 To deplete the photoreceptors, cells were resuspended in 0.5% BSA and stained with
314 CD73-PE antibody (MACS, Catalog: 130-102-616) for 10min at 4C (for each million cells, add
315 98ul 0.5% BSA with 2ul CD73-PE antibody) and washed with 35 ml 0.5% BSA at 4C for 10min.
316 After being stained with Anti-PE microbeads (MACS, Catalog: 130-105-639) (80ul 0.5% BSA and
317 20ul microbeads per each million cells) for 15 min at 4C, cells were washed and resuspended
318 in 0.5% BSA. CD73 negative neuronal cells were enriched by autoMACS Pro Separator (Miltenyi
319 Biotec) DEPLETES mode. Similarly, CD90.1 positive neuronal cells were enriched with CD90.1
320 microbeads (MACS, LOT: 130-094-523; 90ul 0.5% BSA and 10ul CD90.1 microbeads per each
321 million cells) and autoMACS POSSEL-S mode. Cells viability was 87%-94% when checked using
322 DAPI staining under microscope.

323 Guided by 10X manufacturer's protocols (<https://www.10xgenomics.com>), single-cell
324 cDNA library was prepared and sequenced. Briefly, single-cell suspension was loaded on a
325 Chromium controller to obtain single cell GEMS (Gel Beads-In-Emulsions) for the reaction. The
326 library was prepared with Chromium Next GEM single cell 3' kit V2 (10X Genomics) and
327 sequenced on Illumina Novaseq 6000 (<https://www.illumina.com>). Our newly generated
328 single cell data was sequenced at the Single Cell Genomics Core at Baylor College of Medicine.

329

330 ***Data collection and preprocessing of the mouse retinal scRNA-seq***

331 To recover high-quality cells, data samples were processed through a quality control
332 pipeline (<https://github.com/lijinbio/cellqc>). In brief, raw sequencing reads of 10x Genomics
333 were first analyzed by the 10x Genomics Cell Ranger pipeline (version 7.0.1)³⁹ using the mm10
334 genome reference obtained from 10x Genomics (<https://cf.10xgenomics.com/supp/cell-exp/refdata-gex-mm10-2020-A.tar.gz>). Potential empty droplets in the filtered feature count
335 matrices were further detected by dropkick⁴⁰. Background transcripts contamination in the
336 retained true cells were eliminated using SoupX⁴¹. DoubletFinder then was utilized to estimate
337 and exclude potential doublets with high proportions of simulated artificial doublets⁴². In the
338 resulting singlets, we extracted high-feature cells that contain ≥ 300 features, ≥ 500
339 transcript counts, and $\leq 10\%$ of reads mapped to mitochondrial genes.

340
341 In addition to our own data, we have incorporated well-characterized public datasets.
342 Specifically, we have integrated cell-type-enhanced profiling data for amacrine cells
343 (accession: GSE149715)¹², bipolar cells (accession: GSE81904)¹¹, and retinal ganglion cells
344 (accession: GSE133382)⁹. Furthermore, we have included four samples from wild-type mice
345 were also collected from GSE201254 to account for retinal ganglion cells¹³. To account for
346 non-neuronal retinal cells, nine control samples were collected from GSE199317¹⁵. These cell-
347 type specific single-cell datasets form the basis for subclass clustering in our mouse retina
348 reference. To generate the updated transcriptome measurement of the GSE81904 from
349 Shekhar et al., which was derived from the Drop-seq protocol, we applied the Drop-seq
350 pipeline using the source code available at <https://github.com/broadinstitute/Drop-seq>. To
351 ensure consistent gene feature annotation with the Cell Ranger pipeline, we used the gene
352 annotation GTF file from the 10x Genomics mm10 genome reference package during the
353 alignment of Drop-seq reads. In addition, GSE149715, GSE133382, GSE201254, and
354 GSE199317 were also processed from scratch using raw sequencing reads using the 10x
355 Genomics Cell Ranger pipeline (version 7.0.1)³⁹. To incorporate the high-quality cell type
356 annotation of four public datasets, released count matrices and cell labeling were downloaded
357 for meta-analysis. To further eliminate potential multiples in the integrated analysis, Solo
358 doublet detection algorithm was used to identify potential multiples.

359

360 ***Data integration of scRNA-seq datasets***

361 To eliminate technical variations in samples derived from different studies and
362 experiments, 52 samples were integrated to remove the batch effect by scVI⁴³. scVI explicitly

363 formulates the batch effect as a latent variable in the deep generative model of observed
364 expressions. Normalized expression was applied to detect highly variable genes (HVGs) using
365 the Seurat algorithm (flavor: seurat). The “sampleID” was used as the batch key for calculating
366 HVGs and the batch variable in the scVI modeling. The scVI model utilized 2 hidden layers
367 (n_layers: 2) and a 30-dimensional latent space (n_latent: 30). The trained low-dimensional
368 representation was used for cluster detection with the Leiden algorithm ⁴⁴. UMAP of low-
369 dimensional visualization was generated by the Scanpy package ⁴⁵.

370

371 **Cell clustering and cell type annotation**

372 To annotate major classes of cell clusters, we incorporated well-annotated cell labels
373 released from public datasets, i.e., Yan *et al.* for ACs, Shekhar *et al.* for BCs, and Tran *et al.* and
374 Jacobi *et al.* for RGCs. Cells from Yan *et al.* were annotated into 63 AC types. Cells from Shekhar
375 *et al.* were 15 BC types showing in 14 clusters with small numbers of cells annotated as ACs,
376 rod, and cone. Tran *et al.* cells were identified as 45 RGC types. The cell type labels of these
377 well-annotated cells are used to annotate integrated cell clusters. To annotate isolated cell
378 clusters that were isolated from existing cell labels of the public datasets, cluster-specific
379 markers were examined from the top ranked genes generated by the Wilcoxon rank-sum test
380 using the rank_genes_groups() function in the Scanpy package ⁴⁵.

381 To annotate subclass BC, AC, and RGC, subclass-specific cells were isolated and
382 integrated using scVI. The generated low-dimensional embeddings were used to detect
383 clusters using the Leiden algorithm. To determine the optimal number of clusters for
384 subclasses, a two-level clustering approach was applied. In the first level of clustering, various
385 resolutions were tested to achieve clustering without over-clustering in UMAP visualization.
386 The second-level clustering refines the clusters from the first-level clusters by testing various
387 resolutions to achieve optimal clustering without over-clustering on UMAP again. In the first-
388 level, Leiden clusters containing the majority of one type were annotated. When Leiden
389 clusters contained more than one types, cells within the clusters were isolated. Within each
390 subset of isolated cells, Leiden clusters were calculated again using the same low-dimensional
391 embedding. The second-level Leiden clusters were examined for their cell label to determine
392 their cell types.

393 To construct the BC atlas, data samples for BCs were integrated using scVI. Initially, 33
394 clusters were identified, of which 30 could be matched and merged to individual BC types by
395 examining previously generated cell labels and their known marker gene expression ^{11,24}, while
396 the remaining 3 clusters (C30, C31, and C32) were excluded from the analysis as they
397 contained non-BCs from previous annotation labels or had high UMI counts (**Fig. 2a** and
398 **Supplementary Fig. 2a-c**). Consequently, 15 BC types were identified and annotated.

399 To construct the AC atlas, the data integration analysis for ACs using scVI identified a
400 total of 71 clusters, of which 62 clusters could be matched and merged to 49 individual AC
401 types via previous annotation labels and known marker expression. However, 8 clusters were
402 over-clustered that contained two or more previous AC type labels, and one cluster (C70) was
403 excluded from the AC reference due to non-AC cells (**Supplementary Fig. 3c-d**). To further
404 address the 8 remaining over-clustered clusters (**Supplementary Fig. 4a**), we utilized a two-
405 level annotation approach. This involved isolating cells from each cluster and refining the
406 clustering. The two-level annotation allowed the separation of the remaining 14 types: AC11,
407 AC16, AC29, AC42, AC47, AC50, AC53, AC54, AC55, AC56, AC60, AC61, AC62, and AC63
408 (**Supplementary Fig. 4a-c**). This revealed clusters that primarily consisted of RGCs, which have
409 been removed in the integrated AC map (**Supplementary Fig. 4c**). As a result, 63 AC types were
410 identified and annotated.

411 Three AC types, AC16, AC53, and AC62, were identified as dual types expressing both
412 canonical GABAergic and glycinergic receptors in the study by Yan *et al.* AC16, however, was
413 shown as a suspected doublet in their study, alongside AC60. Similarly, our UMAP showed
414 loose cluster formation of AC16 and AC60 in proximity to each other, with relatively high UMI

415 counts (**Fig. 3a** and **Supplementary Fig. 4e**). In addition, our integrated UMAP showed AC53
416 cells spread out in the middle of AC6 cells. Although the AC53 cluster was resolved in the
417 second-level annotation, the loose clustering of AC53 cells is quite apparent. The third dual
418 type, AC62, was also under-clustered and merged with AC42 and AC55. While AC62 was
419 resolved in the second-level annotation, AC62 also appears near its neighboring cluster, AC42,
420 in the UMAP. With very few cells being annotated as dual types in CD90.1 and Ma *et al.*
421 samples, which express high levels of *Thy1* (data not shown), further validations of the dual
422 types are required.

423 To construct the RGC atlas in the MRCA, the integrated analysis identified 54 clusters
424 with an even distribution of cells from different data sources in most clusters (**Supplementary**
425 **Fig. 6a-d**). Out of these clusters, 48 can be mapped and merged into 39 individual RGC types
426 previously identified using marker gene expression and previous annotation labels
427 (**Supplementary Fig. 6a-b**), while five clusters were over-clustered that contained multiple
428 previous RGC types, and one cluster (C8) contained a mixture of several RGC type labels with
429 high UMIs and was excluded from the downstream analysis as multiplets. To annotate the
430 remaining seven types found in the five clusters with multiple labels, the second-level
431 annotation was performed, which resulted in a clear separation of all 46 previously identified
432 RGC types (**Fig. 4a** and **Supplementary Fig.7a-c**).

433

434 **Differentially expressed gene analysis**

435 To identify genes that are differentially expressed between cell types, we generated
436 pseudo-bulk transcriptome of each annotated cell type in individual sample id. We used
437 pyDESEQ2⁴⁶ to compare two clusters or types using the Wald test and identified genes
438 specifically expressed in each cluster or type. Differentially expressed genes are identified
439 under q -value < 0.05 . The Wald statistics ($\log_2\text{FoldChange}$ divided by lfcSE) was used to rank
440 and select the top 10 genes expressed in each type.

441

442 **Data Availability**

443 The raw sequencing reads of sixteen newly generated samples have been deposited
444 at NCBI GEO under the accession GSE243413. The landing page for the MRCA data resources
445 is accessible at <https://rchenlab.github.io/resources/mouse-atlas.html>. Processed cell-by-
446 gene count matrices, along with cell type annotations, are available on Zenodo. Furthermore,
447 both raw and normalized count matrices and cell type annotations are publicly accessible on
448 the CELLxGENE data collection at [https://cellxgene.cziscience.com/collections/a0c84e3f-
449 a5ca-4481-b3a5-ccfda0a81ecc](https://cellxgene.cziscience.com/collections/a0c84e3f-a5ca-4481-b3a5-ccfda0a81ecc). The MRCA is also hosted on the Baylor College of Medicine
450 data portal at <https://mouseatlas.research.bcm.edu>. Additionally, access to the MRCA is
451 provided on the UCSC Cell Browser at <https://retina.cells.ucsc.edu> and the Broad Single Cell
452 Portal.

453

454 **Code Availability**

455 All code used for the MRCA project can be found in the MRCA reproducibility GitHub
456 repository (https://github.com/RCHENLAB/MouseRetinaAtlas_manuscript). The pipeline to
457 process the unpublished and collected public datasets is accessible at
458 <https://github.com/lijinbio/cellqc>.

459

460 **Acknowledgements**

461 We thank Alice Tian for her meticulous proofreading of the manuscript. This project
462 was funded by NIH/NEI R01EY022356, R01EY018571, S10OD032189, Chan Zuckerberg
463 Initiative (CZI) award CZF2019-002425, RRF to R.C.

464

465 **Author contributions**

466 J.L., J.C., X.C., and R.C. conceptualized and designed the study. R.C. supervised the
467 study. X.C. and Y.L. generated scRNA-seq data in this study. J.L., J.M., and S.P. compiled dataset
468 collection. J.L., J.C. and S.P. developed the integrated analysis pipeline and performed the
469 integration and annotation analysis. J.R.S, G.M., and B.J.F. provided public datasets before
470 publishing. N.M.T. provided input for various annotation. All authors wrote, reviewed, and
471 contributed to the manuscript.

472

473 **Competing interests**

474 The authors declare no competing interests.

475

476 References

- 477 1 Masland, R. H. The neuronal organization of the retina. *Neuron* **76**, 266-280 (2012).
478 <https://doi.org/10.1016/j.neuron.2012.10.002>
- 479 2 Jeon, C. J., Strettoi, E. & Masland, R. H. The major cell populations of the mouse retina.
480 *J Neurosci* **18**, 8936-8946 (1998).
- 481 3 Grunert, U. & Martin, P. R. Cell types and cell circuits in human and non-human
482 primate retina. *Prog Retin Eye Res*, 100844 (2020).
483 <https://doi.org/10.1016/j.preteyeres.2020.100844>
- 484 4 Vecino, E., Rodriguez, F. D., Ruzafa, N., Pereiro, X. & Sharma, S. C. Glia-neuron
485 interactions in the mammalian retina. *Prog Retin Eye Res* **51**, 1-40 (2016).
486 <https://doi.org/10.1016/j.preteyeres.2015.06.003>
- 487 5 Boulton, M. & Dayhaw-Barker, P. The role of the retinal pigment epithelium:
488 topographical variation and ageing changes. *Eye (Lond)* **15**, 384-389 (2001).
489 <https://doi.org/10.1038/eye.2001.141>
- 490 6 Tang, F. *et al.* mRNA-Seq whole-transcriptome analysis of a single cell. *Nat Methods* **6**,
491 377-382 (2009). <https://doi.org/10.1038/nmeth.1315>
- 492 7 Macosko, E. Z. *et al.* Highly Parallel Genome-wide Expression Profiling of Individual
493 Cells Using Nanoliter Droplets. *Cell* **161**, 1202-1214 (2015).
494 <https://doi.org/10.1016/j.cell.2015.05.002>
- 495 8 Abdelaal, T. *et al.* A comparison of automatic cell identification methods for single-cell
496 RNA sequencing data. *Genome Biol* **20**, 194 (2019). [https://doi.org/10.1186/s13059-](https://doi.org/10.1186/s13059-019-1795-z)
497 [019-1795-z](https://doi.org/10.1186/s13059-019-1795-z)
- 498 9 Tran, N. M. *et al.* Single-Cell Profiles of Retinal Ganglion Cells Differing in Resilience to
499 Injury Reveal Neuroprotective Genes. *Neuron* **104**, 1039-1055 e1012 (2019).
500 <https://doi.org/10.1016/j.neuron.2019.11.006>
- 501 10 Choi, J. *et al.* Spatial organization of the mouse retina at single cell resolution by
502 MERFISH. *Nat Commun* **14**, 4929 (2023). [https://doi.org/10.1038/s41467-023-40674-](https://doi.org/10.1038/s41467-023-40674-3)
503 [3](https://doi.org/10.1038/s41467-023-40674-3)
- 504 11 Shekhar, K. *et al.* Comprehensive Classification of Retinal Bipolar Neurons by Single-
505 Cell Transcriptomics. *Cell* **166**, 1308-1323 e1330 (2016).
506 <https://doi.org/10.1016/j.cell.2016.07.054>
- 507 12 Yan, W. *et al.* Mouse Retinal Cell Atlas: Molecular Identification of over Sixty Amacrine
508 Cell Types. *J Neurosci* **40**, 5177-5195 (2020).
509 <https://doi.org/10.1523/JNEUROSCI.0471-20.2020>
- 510 13 Jacobi, A. *et al.* Overlapping transcriptional programs promote survival and axonal
511 regeneration of injured retinal ganglion cells. *Neuron* **110**, 2625-2645 e2627 (2022).
512 <https://doi.org/10.1016/j.neuron.2022.06.002>
- 513 14 Ma, J. *et al.* Sample multiplexing for retinal single-cell RNA-sequencing. (*in preparation*
514 *for submission*) (2024).
- 515 15 Benhar, I. *et al.* Temporal single-cell atlas of non-neuronal retinal cells reveals
516 dynamic, coordinated multicellular responses to central nervous system injury. *Nat*
517 *Immunol* **24**, 700-713 (2023). <https://doi.org/10.1038/s41590-023-01437-w>
- 518 16 Tarhan, L. *et al.* Single Cell Portal: an interactive home for single-cell genomics data.
519 *bioRxiv* (2023). <https://doi.org/10.1101/2023.07.13.548886>
- 520 17 Koso, H. *et al.* CD73, a novel cell surface antigen that characterizes retinal
521 photoreceptor precursor cells. *Invest Ophthalmol Vis Sci* **50**, 5411-5418 (2009).
522 <https://doi.org/10.1167/iovs.08-3246>
- 523 18 Kay, J. N. *et al.* Retinal ganglion cells with distinct directional preferences differ in
524 molecular identity, structure, and central projections. *J Neurosci* **31**, 7753-7762
525 (2011). <https://doi.org/10.1523/JNEUROSCI.0907-11.2011>

- 526 19 Chintalapudi, S. R. *et al.* Isolation and Molecular Profiling of Primary Mouse Retinal
527 Ganglion Cells: Comparison of Phenotypes from Healthy and Glaucomatous Retinas.
528 *Front Aging Neurosci* **8**, 93 (2016). [https://doi.org:10.3389/fnagi.2016.00093](https://doi.org/10.3389/fnagi.2016.00093)
- 529 20 Lopez, R., Regier, J., Cole, M. B., Jordan, M. I. & Yosef, N. Deep generative modeling
530 for single-cell transcriptomics. *Nat Methods* **15**, 1053-1058 (2018).
531 [https://doi.org:10.1038/s41592-018-0229-2](https://doi.org/10.1038/s41592-018-0229-2)
- 532 21 Bernstein, N. J. *et al.* Solo: Doublet Identification in Single-Cell RNA-Seq via Semi-
533 Supervised Deep Learning. *Cell Syst* **11**, 95-101 e105 (2020).
534 [https://doi.org:10.1016/j.cels.2020.05.010](https://doi.org/10.1016/j.cels.2020.05.010)
- 535 22 Liang, Q. *et al.* Single-nuclei RNA-seq on human retinal tissue provides improved
536 transcriptome profiling. *Nat Commun* **10**, 5743 (2019).
537 [https://doi.org:10.1038/s41467-019-12917-9](https://doi.org/10.1038/s41467-019-12917-9)
- 538 23 Peng, Y. R. *et al.* Molecular Classification and Comparative Taxonomics of Foveal and
539 Peripheral Cells in Primate Retina. *Cell* **176**, 1222-1237 e1222 (2019).
540 [https://doi.org:10.1016/j.cell.2019.01.004](https://doi.org/10.1016/j.cell.2019.01.004)
- 541 24 Chow, R. L. *et al.* Control of late off-center cone bipolar cell differentiation and visual
542 signaling by the homeobox gene *Vsx1*. *Proc Natl Acad Sci U S A* **101**, 1754-1759 (2004).
543 [https://doi.org:10.1073/pnas.0306520101](https://doi.org/10.1073/pnas.0306520101)
- 544 25 Nadal-Nicolas, F. M. *et al.* True S-cones are concentrated in the ventral mouse retina
545 and wired for color detection in the upper visual field. *Elife* **9** (2020).
546 [https://doi.org:10.7554/eLife.56840](https://doi.org/10.7554/eLife.56840)
- 547 26 Raymond, I. D., Vila, A., Huynh, U. C. & Brecha, N. C. Cyan fluorescent protein
548 expression in ganglion and amacrine cells in a thy1-CFP transgenic mouse retina. *Mol*
549 *Vis* **14**, 1559-1574 (2008).
- 550 27 Firth, S. I., Varela, C., De la Villa, P. & Marshak, D. W. Cholecystokinin-like
551 immunoreactive amacrine cells in the rat retina. *Vis Neurosci* **19**, 531-540 (2002).
552 [https://doi.org:10.1017/s0952523802194156](https://doi.org/10.1017/s0952523802194156)
- 553 28 Kerstein, P. C., Leffler, J., Sivyer, B., Taylor, W. R. & Wright, K. M. Gbx2 Identifies Two
554 Amacrine Cell Subtypes with Distinct Molecular, Morphological, and Physiological
555 Properties. *Cell Rep* **33**, 108382 (2020). [https://doi.org:10.1016/j.celrep.2020.108382](https://doi.org/10.1016/j.celrep.2020.108382)
- 556 29 Theofilas, P., Steinhäuser, C., Theis, M. & Derouiche, A. Morphological study of a
557 connexin 43-GFP reporter mouse highlights glial heterogeneity, amacrine cells, and
558 olfactory ensheathing cells. *J Neurosci Res* **95**, 2182-2194 (2017).
559 [https://doi.org:10.1002/jnr.24055](https://doi.org/10.1002/jnr.24055)
- 560 30 Kim, I. J., Zhang, Y., Yamagata, M., Meister, M. & Sanes, J. R. Molecular identification
561 of a retinal cell type that responds to upward motion. *Nature* **452**, 478-482 (2008).
562 [https://doi.org:10.1038/nature06739](https://doi.org/10.1038/nature06739)
- 563 31 Vaney, D. I., Sivyer, B. & Taylor, W. R. Direction selectivity in the retina: symmetry and
564 asymmetry in structure and function. *Nat Rev Neurosci* **13**, 194-208 (2012).
565 [https://doi.org:10.1038/nrn3165](https://doi.org/10.1038/nrn3165)
- 566 32 Rousso, D. L. *et al.* Two Pairs of ON and OFF Retinal Ganglion Cells Are Defined by
567 Intersectional Patterns of Transcription Factor Expression. *Cell Rep* **15**, 1930-1944
568 (2016). [https://doi.org:10.1016/j.celrep.2016.04.069](https://doi.org/10.1016/j.celrep.2016.04.069)
- 569 33 Kolb, H., Linberg, K. A. & Fisher, S. K. Neurons of the human retina: a Golgi study. *J*
570 *Comp Neurol* **318**, 147-187 (1992). [https://doi.org:10.1002/cne.903180204](https://doi.org/10.1002/cne.903180204)
- 571 34 Shekhar, K. & Sanes, J. R. Generating and Using Transcriptomically Based Retinal Cell
572 Atlases. *Annu Rev Vis Sci* **7**, 43-72 (2021). [https://doi.org:10.1146/annurev-vision-](https://doi.org/10.1146/annurev-vision-032621-075200)
573 [032621-075200](https://doi.org/10.1146/annurev-vision-032621-075200)
- 574 35 Young, R. W. Cell differentiation in the retina of the mouse. *Anat Rec* **212**, 199-205
575 (1985). [https://doi.org:10.1002/ar.1092120215](https://doi.org/10.1002/ar.1092120215)

- 576 36 Garg, M. *et al.* Meta-analysis of COVID-19 single-cell studies confirms eight key
577 immune responses. *Sci Rep* **11**, 20833 (2021). [https://doi.org:10.1038/s41598-021-](https://doi.org/10.1038/s41598-021-00121-z)
578 [00121-z](https://doi.org/10.1038/s41598-021-00121-z)
- 579 37 Prazanowska, K. H. & Lim, S. B. An integrated single-cell transcriptomic dataset for
580 non-small cell lung cancer. *Sci Data* **10**, 167 (2023). [https://doi.org:10.1038/s41597-](https://doi.org/10.1038/s41597-023-02074-6)
581 [023-02074-6](https://doi.org/10.1038/s41597-023-02074-6)
- 582 38 Siegert, S. *et al.* Transcriptional code and disease map for adult retinal cell types. *Nat*
583 *Neurosci* **15**, 487-495, S481-482 (2012). [https://doi.org:10.1038/nn.3032](https://doi.org/10.1038/nn.3032)
- 584 39 Zheng, G. X. *et al.* Massively parallel digital transcriptional profiling of single cells. *Nat*
585 *Commun* **8**, 14049 (2017). [https://doi.org:10.1038/ncomms14049](https://doi.org/10.1038/ncomms14049)
- 586 40 Heiser, C. N., Wang, V. M., Chen, B., Hughey, J. J. & Lau, K. S. Automated quality control
587 and cell identification of droplet-based single-cell data using dropkick. *Genome Res*
588 **31**, 1742-1752 (2021). [https://doi.org:10.1101/gr.271908.120](https://doi.org/10.1101/gr.271908.120)
- 589 41 Young, M. D. & Behjati, S. SoupX removes ambient RNA contamination from droplet-
590 based single-cell RNA sequencing data. *Gigascience* **9** (2020).
591 [https://doi.org:10.1093/gigascience/giaa151](https://doi.org/10.1093/gigascience/giaa151)
- 592 42 McGinnis, C. S., Murrow, L. M. & Gartner, Z. J. DoubletFinder: Doublet Detection in
593 Single-Cell RNA Sequencing Data Using Artificial Nearest Neighbors. *Cell Syst* **8**, 329-
594 337 e324 (2019). [https://doi.org:10.1016/j.cels.2019.03.003](https://doi.org/10.1016/j.cels.2019.03.003)
- 595 43 Lopez, R., Regier, J., Cole, M. B., Jordan, M. I. & Yosef, N. Deep generative modeling
596 for single-cell transcriptomics. *Nature Methods* **15**, 1053-1058 (2018).
597 [https://doi.org:10.1038/s41592-018-0229-2](https://doi.org/10.1038/s41592-018-0229-2)
- 598 44 Traag, V. A., Waltman, L. & van Eck, N. J. From Louvain to Leiden: guaranteeing well-
599 connected communities. *Scientific Reports* **9**, 5233 (2019).
600 [https://doi.org:10.1038/s41598-019-41695-z](https://doi.org/10.1038/s41598-019-41695-z)
- 601 45 Wolf, F. A., Angerer, P. & Theis, F. J. SCANPY: large-scale single-cell gene expression
602 data analysis. *Genome Biol* **19**, 15 (2018). [https://doi.org:10.1186/s13059-017-1382-](https://doi.org/10.1186/s13059-017-1382-0)
603 [0](https://doi.org/10.1186/s13059-017-1382-0)
- 604 46 Muzellec, B., Telenczuk, M., Cabeli, V. & Andreux, M. PyDESeq2: a python package for
605 bulk RNA-seq differential expression analysis. *Bioinformatics* **39** (2023).
606 [https://doi.org:10.1093/bioinformatics/btad547](https://doi.org/10.1093/bioinformatics/btad547)
- 607

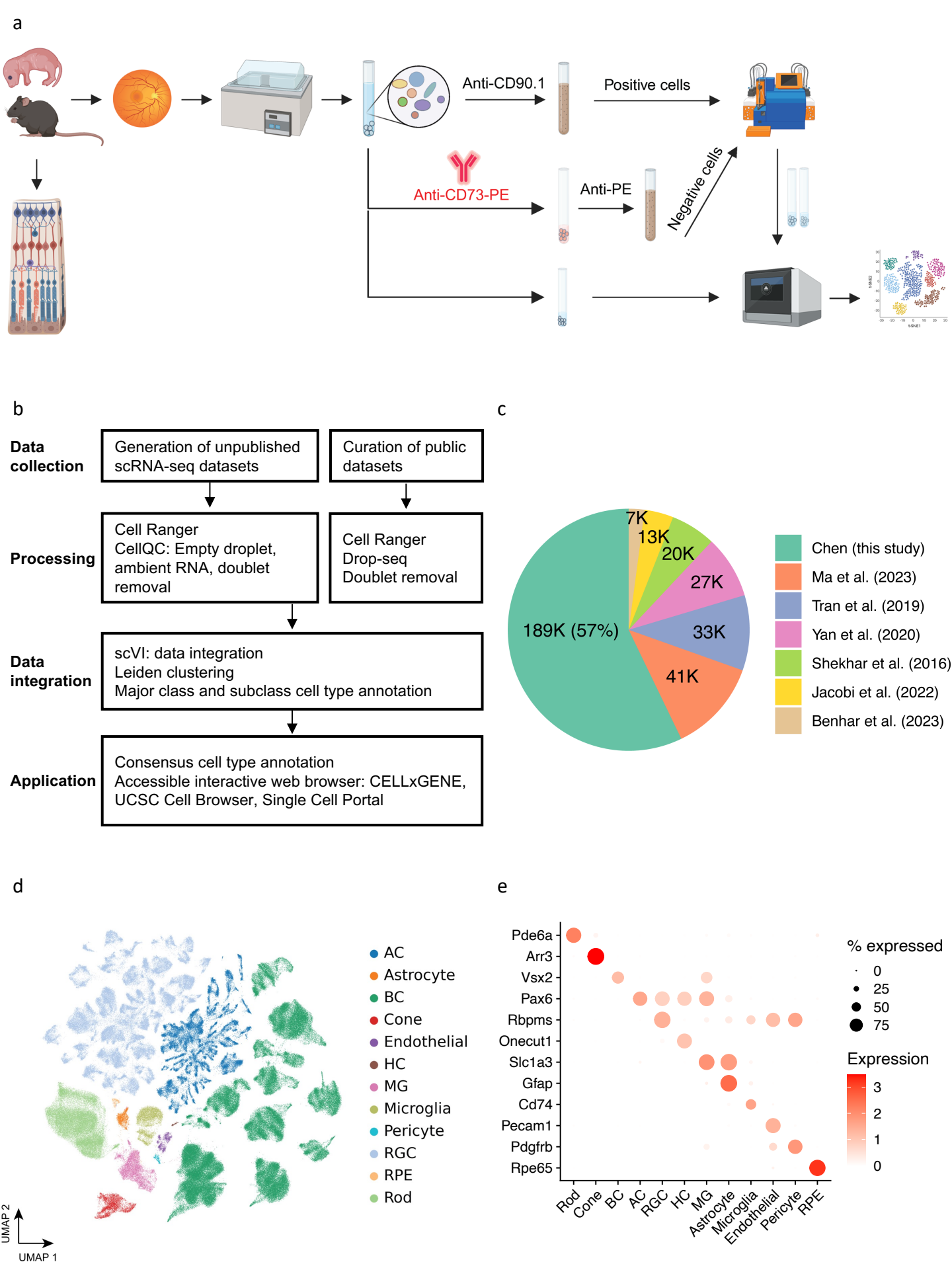


Figure 1. Overview of single cell atlas of the mouse retina

Figure 1. Overview of single cell atlas of the mouse retina

(a) The workflow for generating unpublished scRNA-seq datasets. The data generation process involved using mice aged from P14 to 12 months. Following retina dissection and cell dissociation, single cells were enriched using autoMACS with Anti-CE73-PE antibodies or Anti-CD90.1 beads for specific amacrine, bipolar, and retinal ganglion cells. Subsequently, 10X single-cell RNA sequencing was performed on both the unenriched and enriched single cells. The retained single cells were then utilized in downstream atlas construction. **(b)** The integrated analysis workflow for constructing the MRCA. To construct a comprehensive unified single-cell reference of the mouse retina, we generated 16 unpublished scRNA-seq samples of the mouse retina and incorporated four curated public datasets to enhance specific amacrine, bipolar and retinal ganglion cells. The collected data were processed using the Cell Ranger and CellQC pipeline to produce feature count matrices. Feature counts were then processed to remove estimated empty droplets, ambient RNA, and doublets. The retained cells were integrated using scVI to eliminate batch effects across samples. The trained low-dimensional embeddings were used to calculate cell dissimilarities and identify clustering through a two-level clustering approach. Major class and subclass cell types were annotated using canonical marker genes and public labeling. To facilitate user-friendly access and exploration, the MRCA was deployed on accessible interactive web browsers, including CELLxGENE, UCSC Cell Browser, and Single Cell Portal. **(c)** Pie chart displaying the percentage of cells contributed by each dataset used in the MRCA. **(d)** UMAP visualization of the MRCA colored by major classes. **(e)** Dot plot illustrating the expression of canonical markers for major classes.

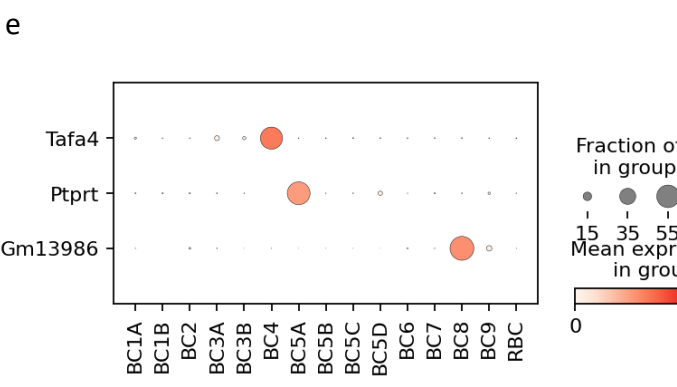
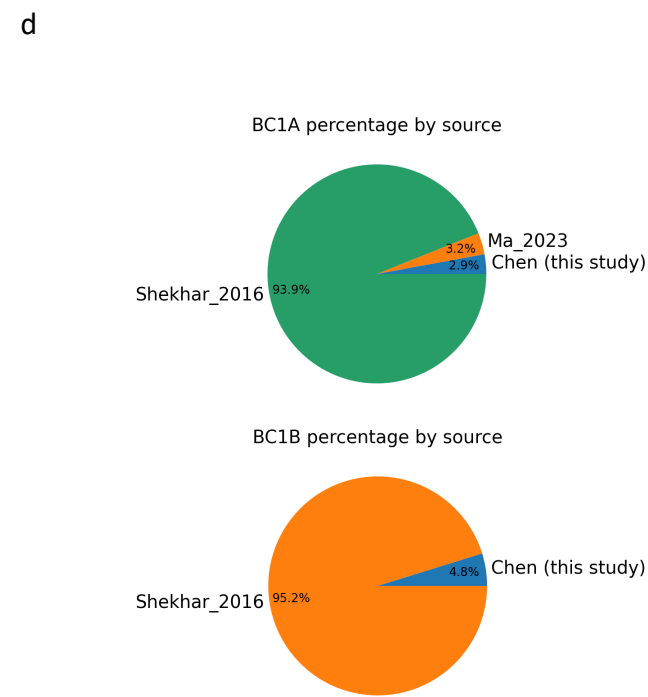
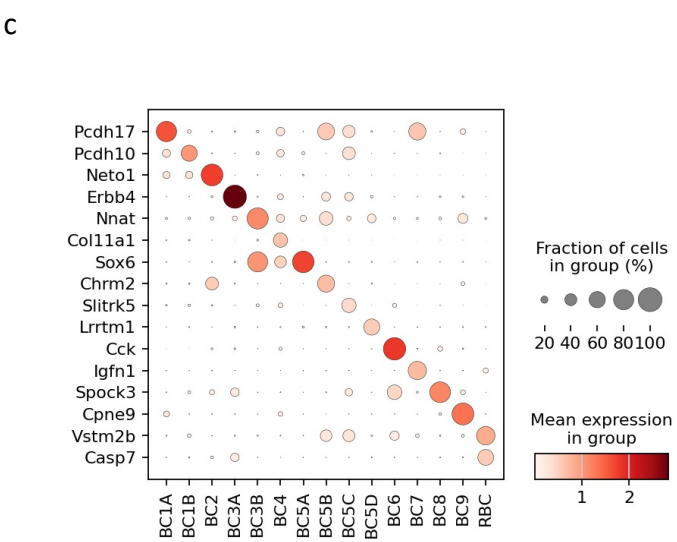
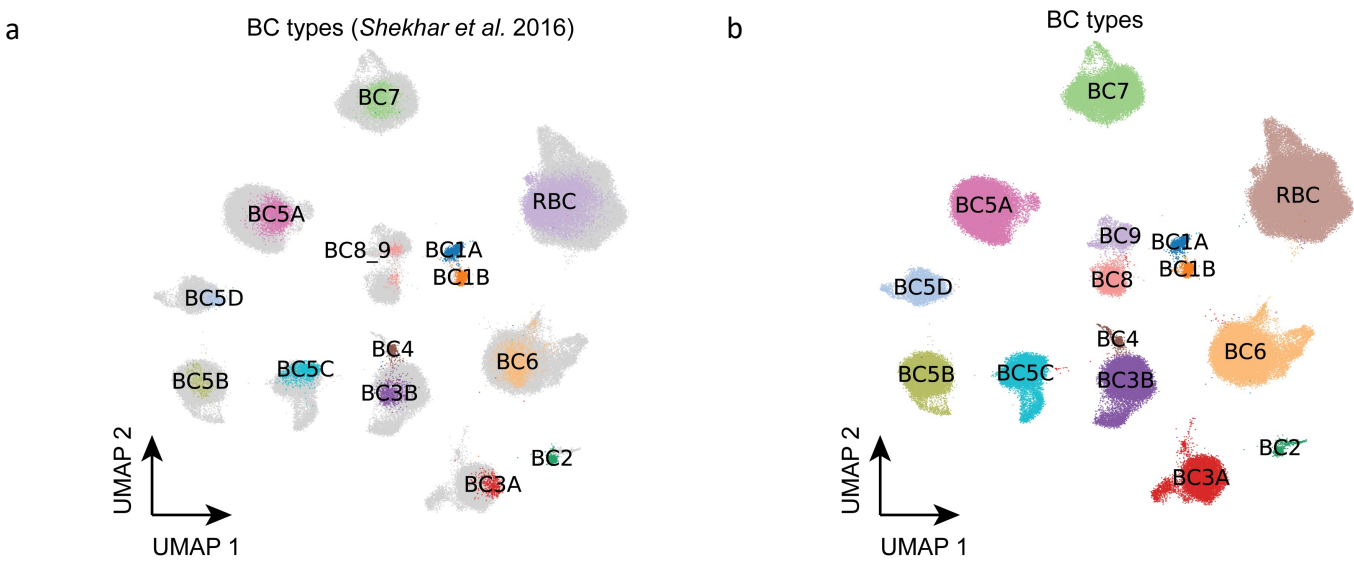


Figure 2. Bipolar cells

Figure 2. Bipolar cells

(a) UMAP visualization of BCs colored by public cell type labels from *Shekhar et al.* 2016. The newly discovered cells without public labeling are colored in gray. **(b)** BCs colored by the 15 annotated annotated cell types. **(c)** Dot plot of BC type marker gene expression in the 15 types. **(d)** Pie chart showing the percentage each data source making up BC1A and BC1B population. **(e)** Dot plot of new markers for three BC types: BC4, BC5A, and BC8. The three new markers exhibit more exclusive expression patterns.

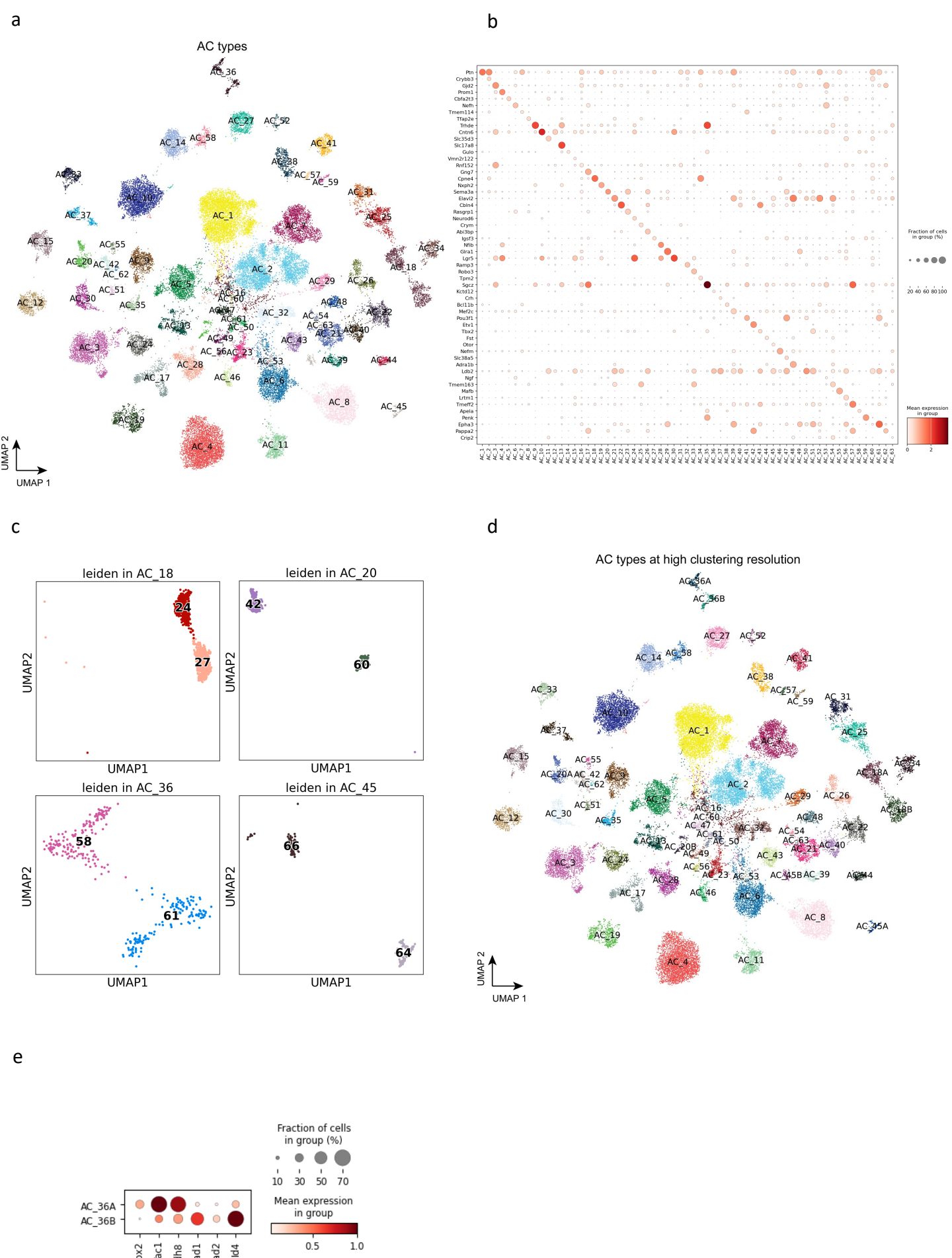


Figure 3. Amacrine cells

Figure 3. Amacrine cells

(a) UMAP visualization of AC cells colored by the annotated types. **(b)** Dot plot of canonical marker gene expression in AC types. **(c)** Four previously under-clustered AC types, i.e., AC18, AC20, AC36, and AC45, are split into two distinct clusters at a high resolution of clustering. **(d)** Visualization of AC cells colored by AC types at a high clustering resolution. **(e)** Dot plot of DEGs expressed in two split clusters for AC_36, stratifying *Gbx2*⁺ AC types in AC_36.

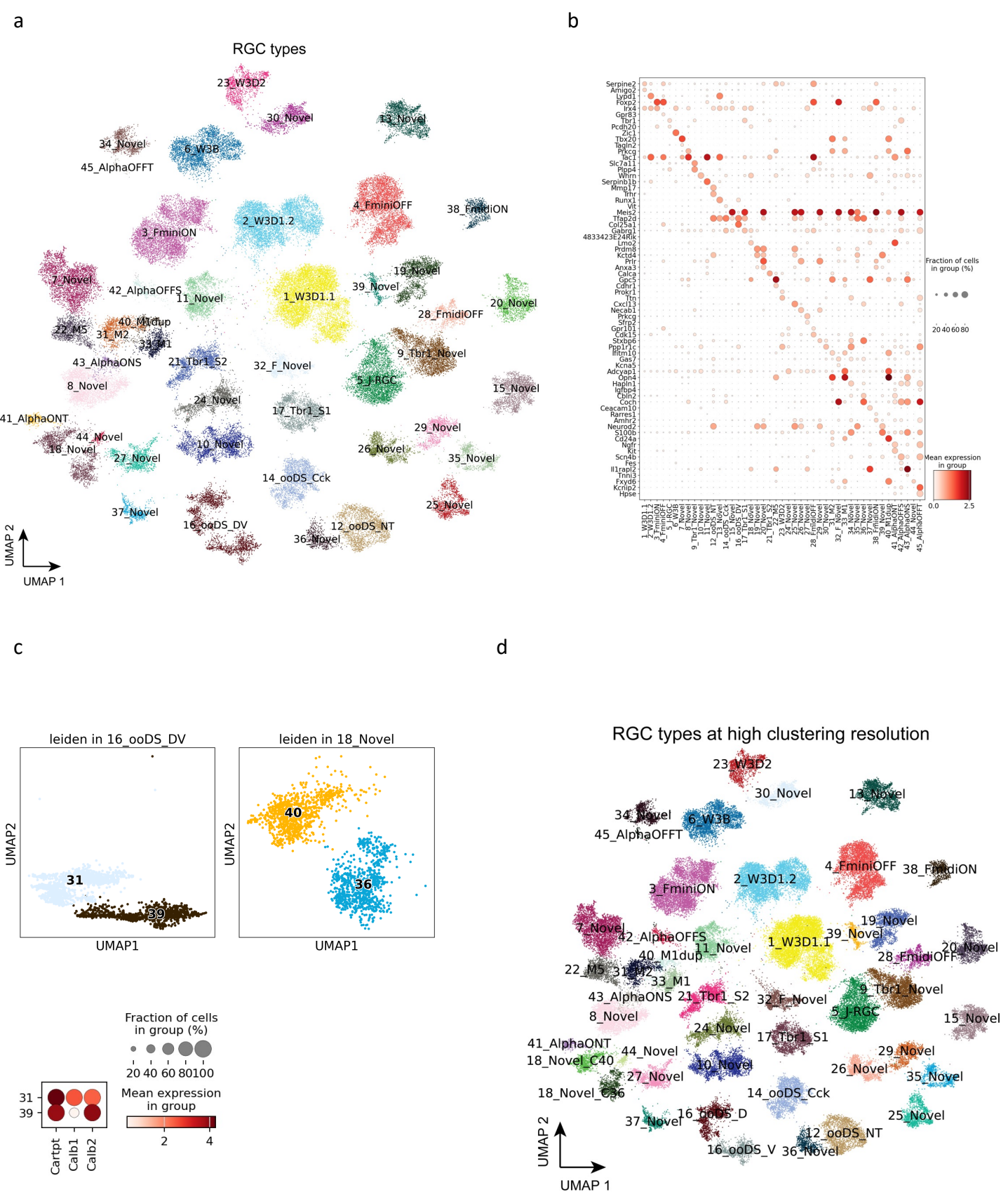


Figure 4. Retinal ganglion cells

Figure 4. Retinal ganglion cells

(a) UMAP visualization of RGC cells colored by the annotated types. **(b)** Dot plot of canonical marker gene expression in RGC types. **(c)** Two previously under-clustered RGC types, i.e., 16_ooDS_DV and 18_Novel, are split into two distinct clusters at a high resolution of clustering. Dot plot of *Calb1* and *Calb2* in the two split clusters of 16_ooDS_DV. **(d)** Visualization of RGC cells colored by RGC types at a high clustering resolution.

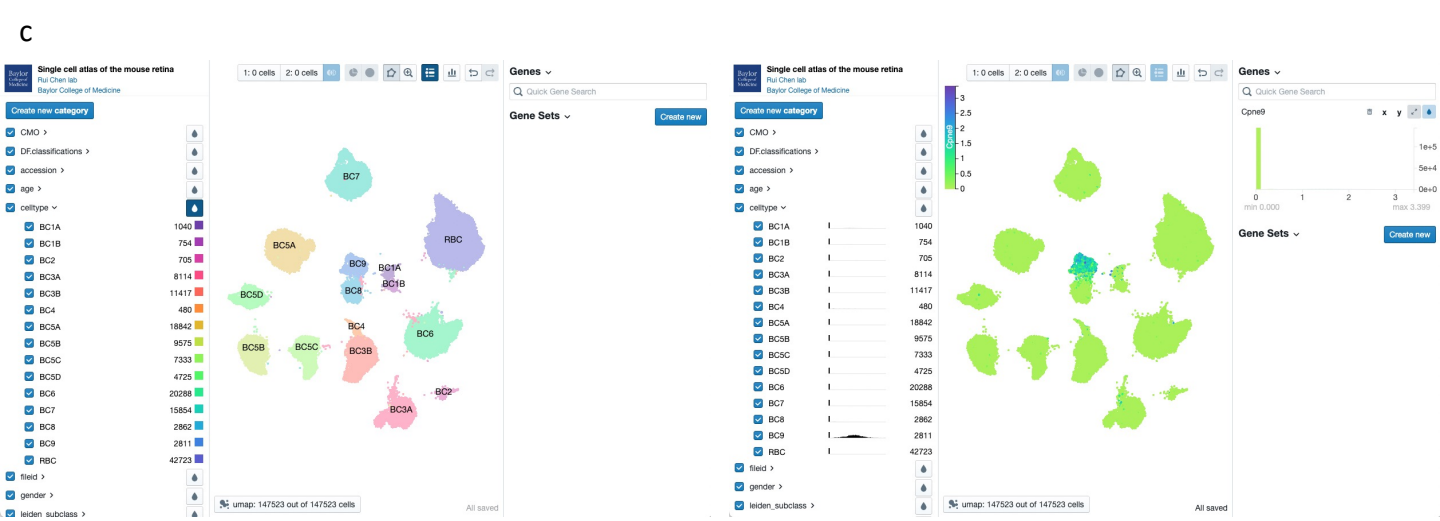
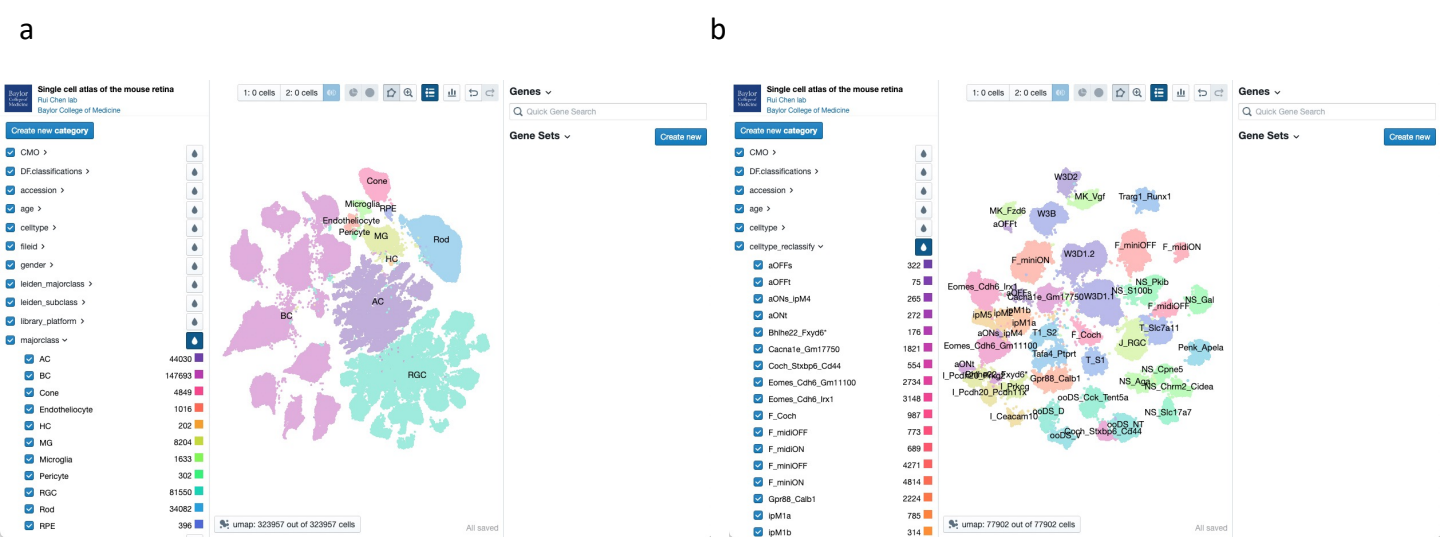


Figure 5. Visualization of MRCA in accessible interactive browsers

Figure 5. Visualization of MRCA in accessible interactive browsers

(a) Visualization of the MRCA in the CELLxGENE browser. The homepage depicts three panels to explore the MRCA. The left panel contains the pre-computed features facilitating the selection of cells by interested categories. The middle panel is the UMAP of the MRCA, colored by the annotated major classes. The right panel allows input of quick gene symbols and gene sets. **(b)** Visualization of the subclass RGC atlas in the CELLxGENE browser. The middle panel depicts RGCs colored by the reclassified names selected in the left panel. **(c)** Visualization of gene expression for a BC9 marker, *Cpne9*, in the BC atlas. The left subfigure shows the BC types, and the right subfigure highlights the normalized gene expression values of *Cpne9* for BC9 type in the middle panel.